Electronic Supplementary Material (ESI) for Nanoscale.

Controlling Layered Ruddlesden-Popper Perovskites via Solvent Additive

*Han Pan [a], Xiaojuan Zhao [a], Xiu Gong [a], Hao Li [b], Xiao Li Zhang [c], Guijie Liang [d], Yan Shen [a], and Mingkui Wang [a,]**

[a] Wuhan National Laboratory for Optoelectronics, School of Optoelectronic Science and Engineering, Huazhong University of Science and Technology, Wuhan 430074, China

[b] Department of Chemistry and Biochemistry, Utah State University, Logan, Utah 84322, United States

[c] State Centre for International Cooperation on Designer Low-Carbon & Environmental Materials, School of Materials Science and Engineering, Zhengzhou University, 450001, China

[d] Hubei Key Laboratory of Low Dimensional Optoelectronic Materials and Devices, Hubei University of Arts and Science, Xiangyang, Hubei 441053, China

Supplementary Discussion

When we use ethanol as the solvent addictive, ethanol will evaporate faster than DMF because of ethanol's higher volatile with lower boiling point. The remnant ethanol cannot complete the dissolution−recrystallization process in the whole perovskite. Thus, the phase distribution with ethanol treated is similar to that without EG treated. In addition, the reason that PL signals from low-n phases in the perovskite with DMSO treated might be explained from two sides. One is that DMSO could increases the nucleation barrier of the high-n phases. If we spin coating precursor solution in RT, the perovskite perfectly self-assemble into thermodynamically favorable low-n phases. The other may be that although sufficient DMSO remained in the after-spin-coating perovskite could induce the Ostwald ripening process, mass transport of the dissolved parts contain the whole perovskite components because DMSO possesses high solubility to both PbI_2 and organic components. Hence, the process cannot largely change the phases and only promotes the small-sized grains to dissolve and redeposit onto the surface of larger particles. Therefore, in the solvent additive-induced Ostwald ripening process to form a uniform phase distribution of RP perovskites, we should select the solvent additive with selective solubility to organic parts, and less volatile with higher boiling points than DMF.

Experimental Section

PbO (99.9%), hydroiodic acid (57 wt.% in H_2O, distilled, stabilized, 99.95%), and hypophosphorous acid solution (50 wt.% in H_2O) were purchased from Sigma-Aldrich and used as received. 2-(4-fhlorophenyl)ethylamine were purchased from Innochem Technology Corp. and used as received.

Synthesis of Cl-PEAI and MAI: hydroiodic acid (12.3 g, 0.055 mol) reacted with 2-(4-Chlorophenyl)ethylamine (7.8 g, 0.05 mol.) for 2 hours under ice bath. The crude product was separated out by evaporating the solvent under reduced pressure. White crystals were obtained after washed with diethyl ether, recrystallized in ethanol and drying at 60 °C overnight in a vacuum.

The preparation steps of CH3NH3I (MAI) were same as the above, only changed the

2-(4-Chlorophenyl)ethylamine to the methylamine (40 wt% in methanol).

The perovskite precursor solutions were prepared by mixing Cl-PEAI, MAI and PbI2 in anhydrous DMF (99.9%) with a molar ratio of 2:3:4. The concentration of $Pb2^{+}$ is 0.6 M. Then ethylene glycol with different volume ratio was added into the perovskite solutions. The mixture solutions were stirred at 70 °C for 30 min in N2 glove box.

Device fabrication

The ITO glass was sequentially cleaned with detergent, deionized water, acetone and ethanol, and then treated in UV-ozone for 30 min. A 40 nm thick PEDOT:PSS (Baytron PVP Al 4083) was spincoated onto the FTO substrate at 4500 rpm for 40 s and annealed at 140 °C for 10 min in air. After perovskite films were spin-coated at 3000 rpm for 45 s and annealing for certain time, $PC_{61}BM$ (20 $mg{\cdot}mL^{-1}$ in chlorobenzene) and BCP (0.5 $mg{\cdot}mL^{-1}$ in isopropanol) were sequentially coated at 2000 rpm for 40 s and 4000 rpm for 40 s, respectively. Finally, 100 nm Ag was deposited by thermal evaporation.

Characterization

XRD measurements were performed with a Shimadzu XRD-6100 diffractometer with Cu Kα radiation. Single-crystal X-ray diffraction data were collected using 39 XtaLAB PRO MM007HF Cu with Cu Kα radiation. All structures were solved by the APEX3 software. The surface morphology of films and energy dispersive spectrometer images were characterized with FEI Nova Nano SEM 450. Visible absorption spectra were recorded using a PerkinElmer Lambda1050 spectrophotometer. The steady-state photoluminescence (PL) spectrum was measured using Horiba Jobin Yvon system with an excitation laser beam at 532 nm and a repetition rate of 76 MHz. The time-resolved luminescence decays were obtained with time-correlated single photo counting system (PicoHarp 300, PicoQuant GmbH). The excitation light source was Ti:Sapphire laser (Mira 900, Coherent; 76 MHz, 130 fs). UPS and XPS measurements were performed by a Kratos AXIS Ultra-DLD ultra-high-vacuum photoemission spectroscopy system with an Al Kα radiation source. The film thickness was measured with a profile-meter (Veeco Dektak 150). The photocurrent-voltage (J-V) characteristics of Cl-$PEA_2MA_3Pb_4I_{13}$ solar cells were obtained by a Keithley model 2400 digital source meter. A xenon light source solar simulator (450 W, Oriel, model 9119) with AM 1.5G

filter (Oriel, model 91192) was used to give an irradiance of 100 mW cm-2 at the surface of the solar cells. The incident photon conversion efficiency (IPCE) measurement was obtained with alternating current (AC) model (130 Hz).

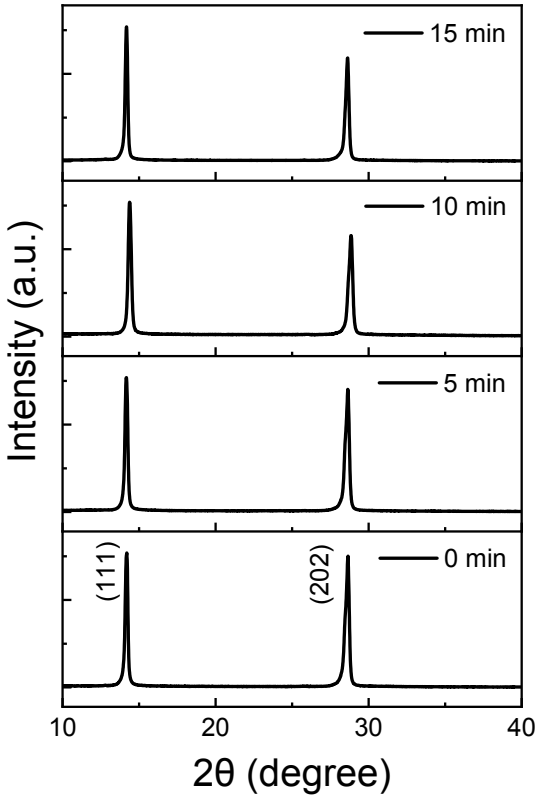

Figure S1. XRD patterns of $(ClPEA)_2MA_3Pb_4I_{13}$ perovskite films without EG treated in a large-angle range.

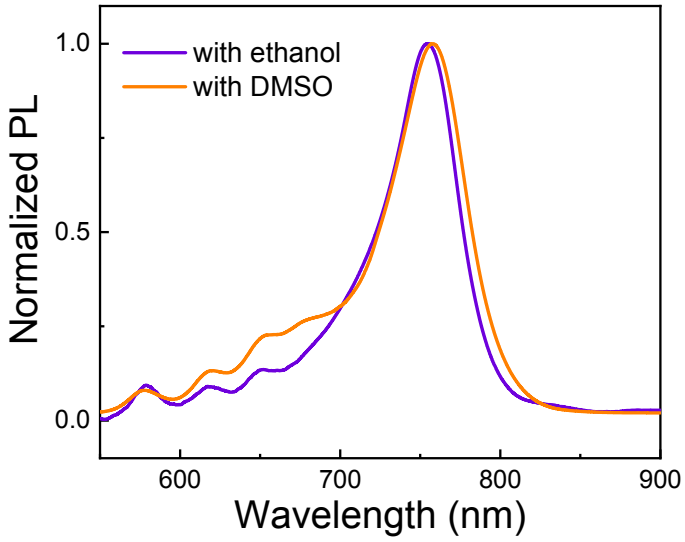

Figure S2. Steady-state PL spectra of $(ClPEA)_2MA_3Pb_4I_{13}$ perovskite films with ethanol or DMSO treated from back side.

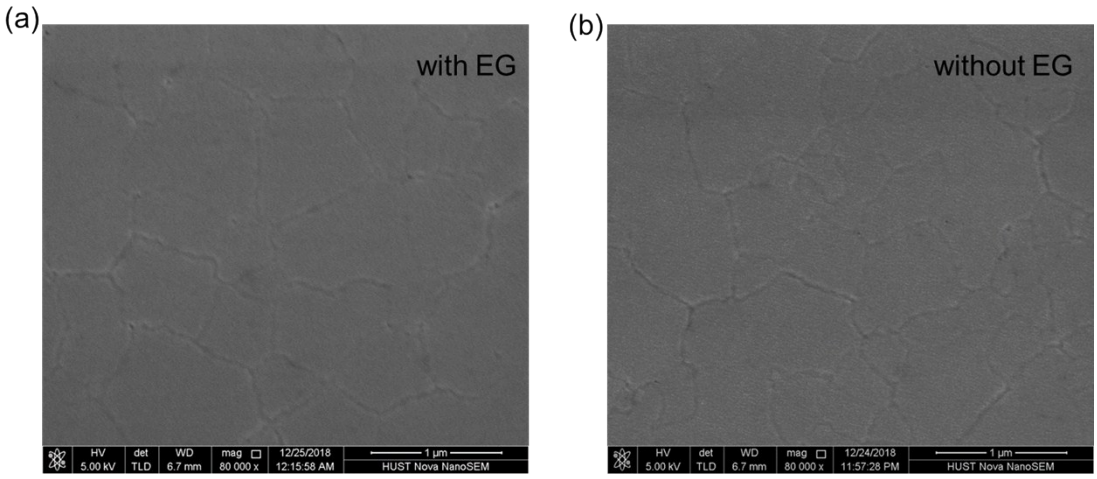

Figure S3. Top-view SEM images of $(ClPEA)_2MA_3Pb_4I_{13}$ perovskite films with and without EG treated on ITO/PEDOT:PSS substrate.

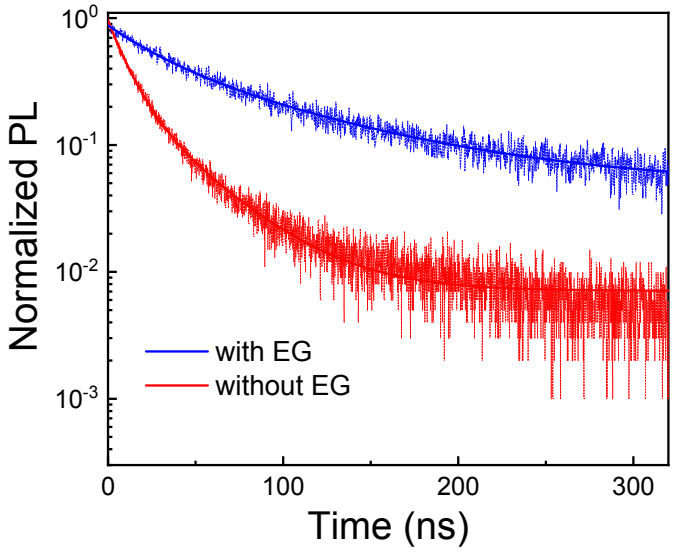

Figure S4. PL decay profiles of $(ClPEA)_2MA_3Pb_4I_{13}$ perovskite films with and without EG treated on the glass substrate

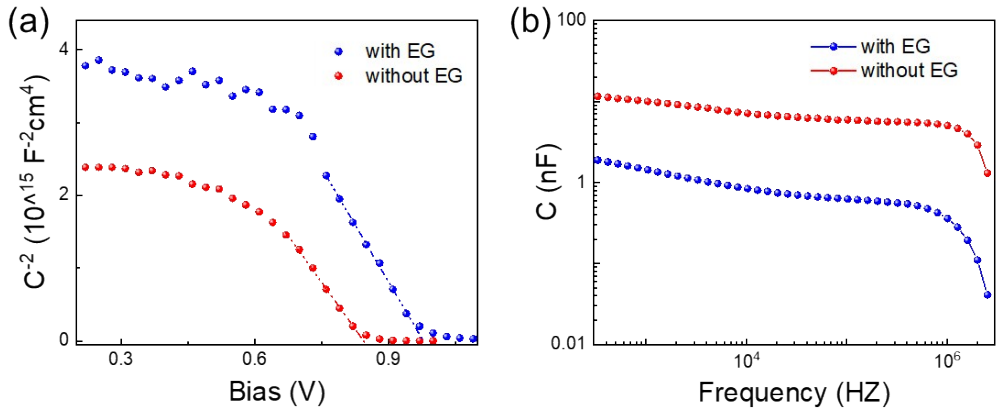

Figure S5. (a) C^{-2}-V characteristics under dark condition, (b) frequency–capacitance *(f–C)* of solar cells with and without EG treated.

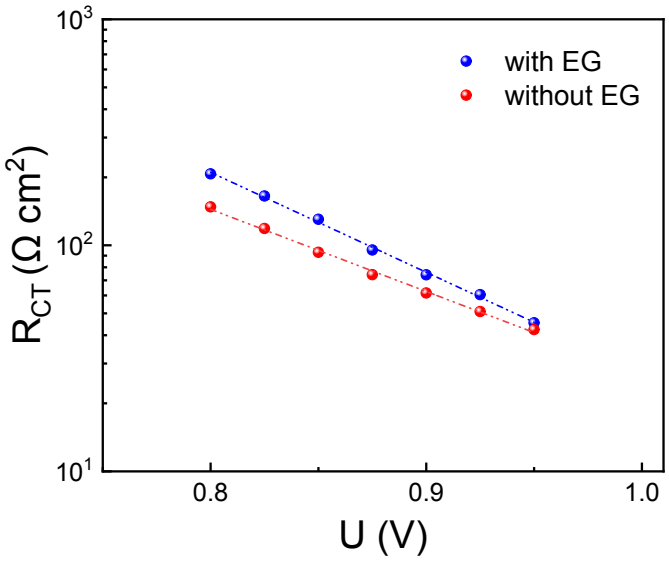

Figure S6. Recombination resistance (R_{rr}) of the devices with and without EG treated by fitting the data from electronic impedance spectroscopy measurements.

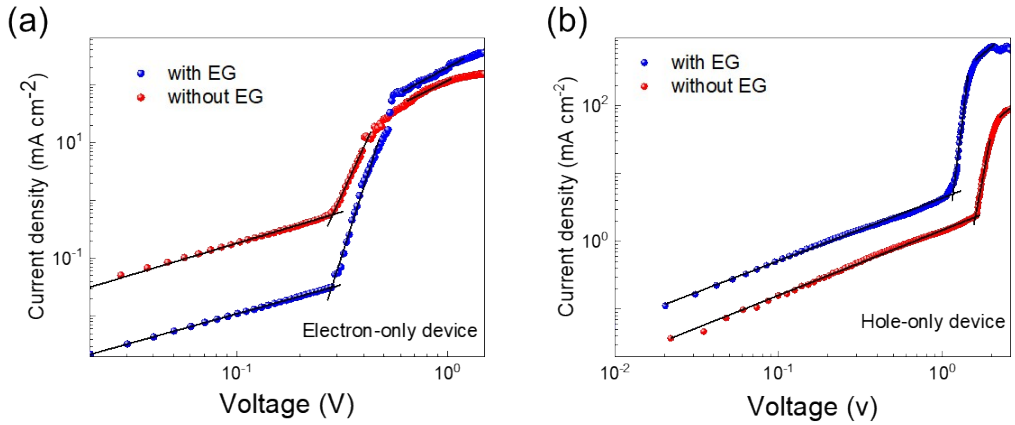

Figure S7. Dark *J–V* measurements of (a)electron- and (b) hole-only devices $(ClPEA)_2MA_3Pb_4I_{13}$ perovskites.

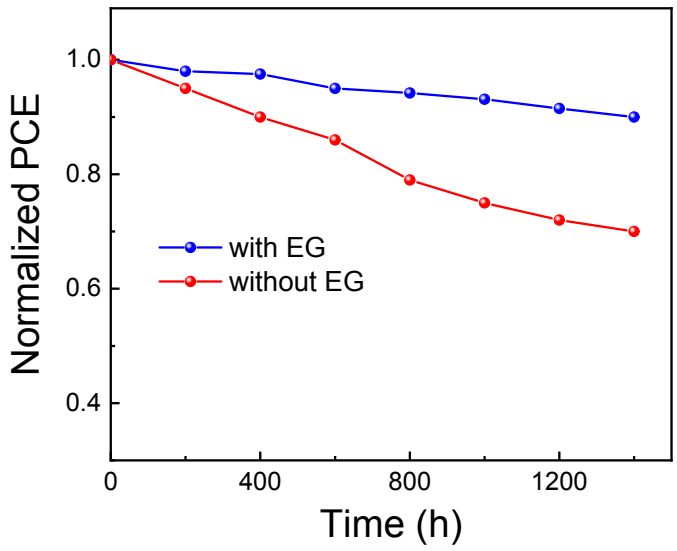

Figure S8. Normalized PCEs versus time for the devices with and without EG treated.

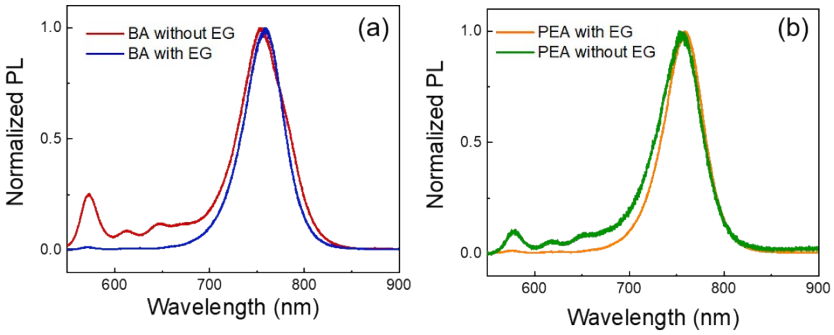

Figure S9. Steady-state PL spectra of (a) $BA_2MA_3Pb4I_{13}$ devices and (b) $PEA_2MA_3Pb_4I_{13}$ devices with and without EG treated from back (glass) side.

Table S1. The photovoltaic parameters of the $(ClPEA)_2MA_3Pb_4I_{13}$-based solar cells with various amounts of EG.

Device	VOC (V)	JSC (mA·cm-2)	FF (%)	PCE (%)	PCE_{AVE} (%)
0	0.94	12.41	67.8	7.91	7.56±0.35
1%	0.96	13.90	69.5	9.27	8.95±0.30
2%	1.01	15.46	70.5	11.01	10.89±0.12
3%	0.99	14.94	68.2	10.07	9.90±0.17
4%	0.88	11.62	59.3	6.06	5.64±0.42

PCE_{AVE} presents the average PCEs of 30 devices.

Table S2. The photovoltaic parameters of the device with and without EG treated with different scan directions.

Device	Scan direction	V_{OC} (V)	J_{SC} (mA·cm^{-2})	FF (%)	PCE (%)	PCE_{AVE} (%)
with EG	RS	1.01	15.456	70.5	11.01	10.89±0.19
	FS	1.00	15.432	70.0	10.80	10.64±0.16
without EG	RS	0.94	12.408	67.8	7.91	7.56±0.35
	FS	0.91	12.396	63.6	7.17	6.94±0.23

PCE_{AVE} presents the average PCEs of 30 devices.

Table S3. The photovoltaic parameters of the device based on BA ($BA_2MA_3Pb4I_{13}$) and PEA($PEA_2MA_3Pb_4I_{13}$) perovskites with and without EG treated with different scan directions.

Device	without/ with EG	VOC (V)	JSC ($mA \cdot cm^{-2}$)	FF (%)	PCE (%)	PCE_{AVE} (%)
BA	without	0.95	12.01	59.5	6.79	6.41±0.38
	with	0.97	14.12	63.2	8.65	8.32±0.33
PEA	without	0.93	12.27	65.7	7.50	7.25±0.25
	with	0.98	14.35	69.4	9.76	9.47±0.29

PCE_{AVE} presents the average PCEs of 20 devices.